6) See if the following equation is satisfied:

$$\int_{\omega=-90^\circ}^{\omega=0} f(\beta)d\omega = \int_{\omega=0}^{\omega=90^\circ} f(\beta)d\omega \qquad (39)\S$$

If Eq. (39) is not satisfied, repeat the procedure for a different β_i value.

For the correct value of β_i, the nondimensional coordinates x/R_m and y/R_m of the meridian of the toroid can be found from Eqs. (40):

$$x/R_m = (\sin\beta_m/\sin\beta) - 1$$

$$\frac{y}{R_m} = \mp\sin\beta_m \int_0^\omega f(\beta)d\omega \qquad (40)$$

plus sign for $x > 0$ or $\beta < \beta_m$
minus sign for $x < 0$ or $\beta > \beta_m$

If R_i and R_o are given numerically, the radius R_m can be determined from Eq. (27), and the coordinates x and y can be calculated dimensionally from Eqs. (40).

In calculating values of ω (see step 4) for various values of the angle β, it is preferable to get equally spaced values of ω rather than of β, in order to get approximately equally spaced points on the meridional section of the toroid; this also facilitates the integrations shown on both sides of Eq. (39) since Simpson's rule can be used most effectively. Provision for equally spaced values of ω, however, requires two or three trials per value because β cannot be expressed as an explicit function of ω.

Numerical Example: R_i = 13 ft, R_o = 20 ft

The preceding method was applied to a toroid whose radii on the equatorial plane are 13 and 20 ft. The solution is given in a tabular form, which includes only the last step of approximation. As shown at the bottom of Table 1, Eq. (39) is satisfied only approximately because $I_1 - I_2 = 0.3900 - 0.3890 = 0.0010$ instead of zero. The accuracy, however, is considered satisfactory. Coordinates x and y were calculated from Eqs. (40), and corresponding values along with β values are given in a table in Fig. 3, where half the meridional section of the toroid also is plotted.

The most remarkable conclusion is that the meridional section of the toroid is very nearly circular, and for all practical purposes it can be taken as such. This conclusion, however, must not be generalized before other meridional sections are plotted for more R_i/R_o values. It can be seen easily that a circular torus does not lend itself to a filament-winding process because the stress ratio at points around a meridian varies in a way incompatible with the rate of change of the wrap angle. The numerical example, however, shows that a very nearly circular torus ($R_i/R_o = 0.65$) can be filament wound if the filaments start at a wrap angle $\beta_i = 42^\circ$ on the inner equator. An explanation for this lies on the sensitivity of the circumferential stresses in a torus. In fact, if general equations for the principal stresses are written for a toroid of elliptical meridional section, it can be seen that it does not take much eccentricity in order for the circumferential stress pattern to change considerably.[3]

§ This is an equivalent equation of the condition $y_{(x=x_i)} = y_{(x=x_o)}$, which is given by Eq. (35). In fact, substituting Eq. (37) into Eq. (34) and simplifying results in

$$F(\beta) = \cos\beta \tan\omega/\sin^2\beta \qquad (i)$$

Differentiating Eq. (37) and simplifying yields

$$\cos\omega d\omega = \frac{\sin^2\beta_m \sin^2\beta - 2\sin^2\beta_m \cos^2\beta - \sin^4\beta}{\sin^3\beta \cos^2\beta} d\beta \qquad (ii)$$

Dividing Eqs. (37) and (ii) yields

$$\cot\omega\, d\omega = \frac{\sin^2\beta_m \sin^2\beta - 2\sin^2\beta_m \cos^2\beta - \sin^4\beta}{\sin\beta \cos\beta(\sin^2\beta_m - \sin^2\beta)} d\beta \qquad (iii)$$

Solving Eq. (iii) for $d\beta$ and multiplying the resulting equation and Eq. (i) gives

$$F(\beta)d\beta = \frac{\cot^2\beta}{\sin\beta} \frac{1 - (\sin\beta_m/\sin\beta)^2}{1 + (\sin\beta_m/\sin\beta)^2(2\cot^2\beta - 1)} d\omega$$

which reduces to $F(\beta)d\beta = f(\beta)d\omega$ if Eq. (38) is taken into account. From the last equation, the equivalence between Eqs. (35) and (39) is obvious.

References

[1] Timoshenko, S., *Strength of Materials* (D. Van Nostrand Co. Inc., New York, August 1941), 2nd ed., Part II, p. 160.

[2] Greenhill, A. G., *The Applications of Elliptic Functions* (Dover Publications Inc., New York), p. 96.

[3] Turner H. M., "Design parameters for elliptical toroidal pressure vessels," Aerospace Eng. 21 (November 1962).

Flow Separation in Overexpanded Contoured Nozzles

M. Arens*

Technion-Israel Institute of Technology, Haifa, Israel

Reference 1 presented some data on separation due to overexpansion in contoured nozzles. Unfortunately, the experimental data are presented in a system of coordinates which bears little relation to the parameters describing the separation phenomenon, and, therefore, the significance of the results is masked This defect is mentioned by the authors of Ref. 1.

In Refs. 2–5, it has been shown that the significant parameters describing flow separation in overexpanded nozzles are the separation pressure ratio, i.e., the ratio of the wall pressure at the separation point to ambient pressure, and the separation Mach number. It also has been shown that all available experimental data on two-dimensional and conical nozzles of half angles up to 30° correlate adequately when plotted as a function of the Mach number in the separation plane. Reference 4 introduces a simple theory to account for the variation of the separation pressure ratio as a function of the Mach number and the specific heat ratio.

In attempting to relate contoured nozzle data to those of straight-walled nozzles, the following essential differences should be borne in mind:

1) *There are differences in the pressure gradient along and normal to the nozzle wall.* Information available to date indicates that variations in the longitudinal positive pressure gradient have a negligible effect on the separation pressure rise. The effect of a normal pressure gradient has not been investigated. It is to be expected that a normal gradient will either delay or cause earlier separation, depending on the sense of the gradient in the vicinity of the separation point.

2) *Because of the curvature of the nozzle wall, the geometry of the separated region generally differs from that encountered in straight-walled nozzles.* This difference may account for variations in the pressure rise occurring in the separated region.

Figure 1 presents experimental data for the ratio of pressure at the separation point to ambient pressure for contoured nozzles. The data are taken from Refs. 1, 6, and 7. The correlation for straight-walled nozzles of Ref. 4 is indicated also. The considerable scatter is probably due to the range of pressure gradients prior to separation and different separated region geometries that are encountered in contoured

Received May 22, 1963.

* Associate Professor, Department of Aeronautical Engineering. Member AIAA.

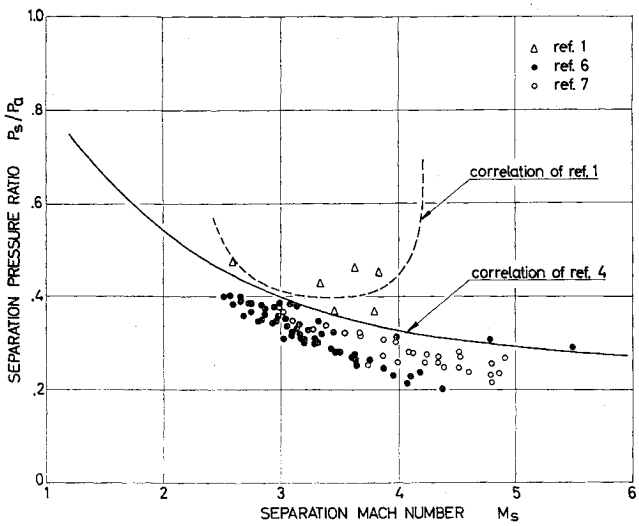

Fig. 1 Separation pressure ratio for contoured nozzles.

nozzles. The overall trend is similar to that for straight-walled nozzles. The correlation suggested in Ref. 1, transformed to the coordinates of Fig. 1, is shown also. It clearly is not adequate.

References

[1] Roschke, E. J. and Massier, P. F., "Flow separation in a contour nozzle," ARS J. **32**, 1612–1613 (1962).

[2] Arens, M. and Spiegler, E., "Separated flow in overexpanded nozzles at low pressure ratios," Bull. Res. Council Israel **11C**, 45–55 (1962).

[3] Arens, M., "Turbulent shock-wave boundary layer separation and overexpanded nozzle flow," *Proceedings of the XIIIth International Astronautical Congress, Varna, Bulgaria, 1963* (to be published).

[4] Arens, M. and Spiegler, E., "Shock induced boundary layer separation in overexpanded conical exhaust nozzles," AIAA J. **1**, 578–581 (1963).

[5] Arens, M., "The shock position in overexpanded nozzles," J. Roy. Soc. (London) **67**, 268–269 (1963).

[6] Ahlberg, J. H., Hamilton, S., Migdal, D., and Nilson, E. N., "Truncated perfect nozzles in optimum nozzle design," ARS J. **31**, 614–620 (1961).

[7] Farley, J. M. and Campbell, C. E., "Performance of several method of characteristics exhaust nozzles," NASA TN D-293 (1960).

Offset-Aim Target Seeker Technique for Interplanetary Ballistic Trajectories

MARTIN A. KROP* AND HERMAN F. MICHIELSEN†
Lockheed Missiles and Space Company, Sunnyvale, Calif.

THE determination of the exact initial conditions for a precise interplanetary ballistic trajectory is a problem met frequently in astrodynamic studies. A common approach is to linearize the equations of motion, generate the elements of a coefficient matrix, solve for a set of changes, and iterate until a satisfactory trajectory is attained. This note presents an iteration scheme, more effective and involving fewer computations than the matrix approach.

Received March 19, 1963. This work was sponsored in part by the NASA George C. Marshall Space Flight Center, under Contract NAS 8-2469, and in part by the Independent Research Program of Lockheed Missiles and Space Company.

* Research Specialist, Flight Mechanics, Mechanical and Mathematical Sciences Laboratory. Member AIAA.

† Senior Member, Flight Mechanics, Mechanical and Mathematical Sciences Laboratory. Member AIAA.

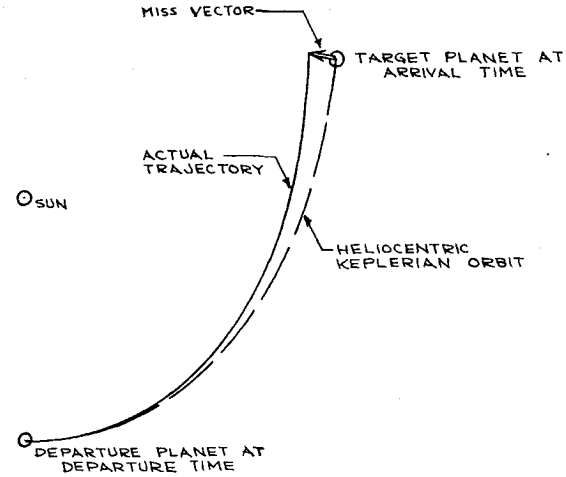

Fig. 1a Trajectory geometry; first pass.

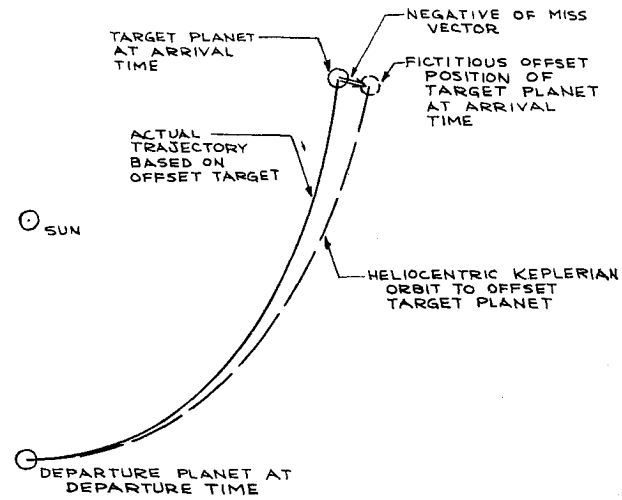

Fig. 1b Trajectory geometry; iterative pass.

The nature of the problem to be solved is characterized as follows: determine the initial conditions for a precise interplanetary ballistic flight that leaves and arrives on specified dates; the trajectory departs along a vertical launch‡ or from a parking orbit and arrives with a vertical impact or into a specified orbit about the target planet; and the trajectory integration includes the usual solar system perturbations.

Description of the Technique

The iteration scheme employs an offset-aim technique to converge on the required initial conditions. Approximate launch conditions are computed from the two-body heliocentric unperturbed Keplerian orbit equations. With these launch conditions an exact trajectory, including all perturbations, is calculated to the vicinity of the target planet, and the miss distance vector is noted; this step is depicted in Fig. 1a. Then, the arrival end of the heliocentric Keplerian orbit is offset by the negative of this miss vector, and the launch conditions are recomputed for the next exact trajectory integration as shown in Fig. 1b. The process is repeated, and the initial conditions are improved until the miss vector is reduced to a tolerable size. The miss distance vector at the target planet is the miss measured relative to the incoming planetocentric hyperbolic asymptote, similar to the vector $\bar{B}$ of Kizner.[1] This vector behaves in a nearly linear manner

‡ Although a vertical launch admittedly is not realistic for flight planning, it is useful for parametric studies.